JOURNAL OF GEOPHYSICAL RESEARCH, VOL. 96, SUPPLEMENT, PAGES 19,085–19,100, OCTOBER 30, 1991

Voyager 2 Electron Observations in the Magnetosphere of Neptune

MING ZHANG[1]

Department of Physics and Center for Space Research, Massachusetts Institute of Technology, Cambridge

JOHN D. RICHARDSON

Center for Space Research, Massachusetts Institute of Technology, Cambridge

EDWARD C. SITTLER, JR.

Laboratory for Extraterrestrial Physics, NASA Goddard Space Flight Center, Greenbelt, Maryland

This paper describes electron data obtained during the Neptune encounter by the Voyager 2 plasma science experiment. We derive the densities and temperatures of low-energy (10-5950 eV) electrons and the electrostatic potential of the spacecraft near Neptune. The data indicate that the escape of charged particles from Triton and the local ionization of atoms in the neutral torus originating from Triton are the major plasma sources. We infer that this neutral torus of hydrogen atoms has a density of about 300 cm^{-3} and an inner boundary at 8 R_N. The data near Neptune exhibit signatures suggesting that both precipitation into Neptune's atmosphere and ring absorption are important plasma loss mechanisms. Plasma transport in the magnetosphere appears to be very fast; the diffusion coefficient is $1\times10^{-7}L^3\ R_N^2\ s^{-1}$.

INTRODUCTION

The Voyager 2 encounter with Neptune in August of 1989 revealed that Neptune has a fully developed and complex magnetosphere. Triton, Neptune's major satellite, has an extended atmosphere and ionosphere and injects neutral atoms as well as charged particles into the magnetosphere [*Broadfoot et al.*, 1989; *Yung and Lyons*, 1990]. This produces a neutral torus coincident with Triton's orbit. Ionization of these neutrals would form a plasma torus similar to the Io plasma torus at Jupiter if the magnetic dipole axis of Neptune were approximately aligned with the spin axis. However, the magnetic dipole axis of Neptune is tilted 46° from the spin axis [*Ness et al.*, 1989]. Thus the neutral torus of Triton spans a large range of L shells in the magnetic dipole system. The rate of ionization of neutrals in this torus is longitudinally inhomogeneous, with peak plasma production at longitudes of 170° and 350°, which may result in the formation of two plasma arcs [*Broadfoot et al.*, 1989]. The large tilt of the magnetic dipole also causes the configuration of the magnetosphere to change diurnally, as was the case at Uranus. Since the spin axis of Neptune is nearly perpendicular to the Sun-planet line, the configuration of Neptune's magnetosphere changes from Earthlike to pole-on and back again every Neptunian day [*Belcher et al.*, 1989; *Ness et al.*, 1989].

In this paper we analyze data from the plasma science experiment (PLS) electron measurements and derive the electron densities and temperatures. We compare the electron measurements with PLS ion measurements to find the potential of the spacecraft in the magnetosphere. On the basis of the results of our data analysis, we discuss the Triton neutral torus, magnetospheric plasma transport, and plasma sources and sinks. A companion paper [*Richardson et al.*, this issue] presents results from the PLS positive ion measurements.

INSTRUMENT AND DATA ANALYSIS

Details of the PLS instrument on Voyager were described by *Bridge et al.* [1977]. The electron spectral analysis has been described by *Scudder et al.* [1981], *Sittler* [1983], *Sittler et al.* [1983], and *Sittler et al.* [1987]. The technique for fitting electron spectra using several Maxwellian distribution functions is found in these papers, and here we do not repeat the description of this technique.

Of the four Faraday cup sensors on the PLS instrument, only the side sensor (D cup) measures electron fluxes. Two energy scan modes, the low-energy E1 mode (10–140 eV) and the high-energy E2 mode (10-5950 eV), are employed. Both energy modes consist of 16 contiguous energy channels which are used to obtain differential distributions of the electron flux into the D cup. The first four channels of the E2 mode, which range from 10 to 140 eV, overlap the E1 mode coverage and are not used in our analysis. The sampling scheme used by PLS at Neptune is the same as that used at Uranus and is described in Table 1 of *Sittler et al.* [1987]. The sampling time for each spectrum is 3.84 s for the short-integration (E1-short and E2-short) modes and 15.4 s for the long-integration (E1-long and E2-long) modes. The cycle time of the electron measurement is 96 s. In this paper (unless otherwise stated) we use data from the long-integration time modes. The effective time resolution is 96 s, but this time resolution is further affected by interference associated with spacecraft operation. About one sixth of the electron spectra are not used. The actual time resolution of the electron data used in this paper is about 2 min.

[1]Now at the Enrico Fermi Institute, the University of Chicago, Chicago, Illinois.

Copyright 1991 by the American Geophysical Union.

Paper number 91JA01857.
0148-0227/91/91JA-01857$05.00

Since electron measurements are made in only one cup and the orientation of this cup is fixed in space (except during spacecraft roll maneuvers), angular information about the electron distribution in velocity space is not available. The D cup has a fairly broad angular response with a conical half angle of 30° about the cup look direction. The spectra we obtain are amalgamations of the electron distribution functions with the response function of the Faraday cup. We usually fit the spectra with isotropic Maxwellians [*Sittler*, 1983]; significant departures of the data from this model, as with a large anisotropy or a plasma loss cone distribution, could lead to an inaccurate estimate of plasma parameters. Voyager 2 made a very close approach to Neptune (1.18 R_N; 1 $R_N \equiv$ 24,765 km) and, as a result, the effect of the loss cone on the plasma distribution can be significant, particularly near closest approach. This will be discussed in more detail later.

Another factor affecting the measurements is the spacecraft charging. At Neptune, plasma in the magnetosphere is relatively cold; the thermal electron temperature is less than 10 eV in most regions. A spacecraft potential of the order of a few volts could seriously affect estimates of the electron density. *Scudder et al.* [1981] found an empirical relation between the electron return current to the spacecraft and the spacecraft potential, but this relation is only valid when the potential is positive. Unfortunately, in Neptune's magnetosphere the spacecraft was negatively charged, and another method must be used to derive the electron density and spacecraft potential. This problem is solved using the assumption of spatial charge neutrality [see *Scudder et al.*, 1981; *Sittler and Strobel*, 1987] and the independent calculations of plasma density from the PLS ion measurements [*Richardson et al.*, this issue].

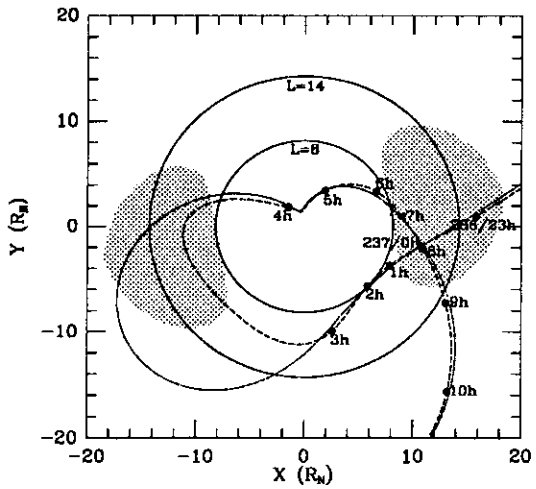


Fig. 1*a*. Voyager 2 trajectory projected along magnetic field lines onto the magnetic equator. Both the OTD (dotted line) and I8E1 (dashed line) field model are used. The magnetic dipole axis is outward from the paper. The positive X axis is in the direction of zero longitude. Two expected plasma arcs are schematically shown by the shaded regions.

TRAJECTORY

Figure 1*a* shows the spacecraft trajectory during the time period when Voyager was in the magnetosphere of Neptune. This is a projection of the trajectory along the magnetic field lines onto the magnetic equator of the offset tilted dipole (OTD). The dipole (Z) axis points out of the page. The X axis is in the direction of 0° planetographic longitude, and the Y axis completes a right-handed coordinate system. In order to compare the different magnetic field models, we plot in Figure 1*a* two trajectory curves; one (dotted line) is calculated using the OTD field model of *Ness et al.* [1989] and the other (dashed line) using the I8E1 field model of *Connerney et al.* [this issue]. Coefficients up to the octupole expansion in the I8E1 field model are used in the calculation because the unresolved terms in the higher-order expansions are not reliable. The distance of each point on the trajectory from the origin corresponds to the L shell of the spacecraft at that same time. Thus this is a polar diagram of L shell and magnetic longitude. Tick marks on the trajectories give the time in day and hour in UT (coordinated universal time at Voyager).

The two curves agree quite well except between 237/0030 (day/hour minute) and 237/0345 UT, when the spacecraft was at high magnetic latitudes and near Neptune. Figure 1*b* shows the magnetic latitude in the OTD model and radial distance of the spacecraft as a function of time. The three magnetic equator crossings are at 237/0023 UT, 237/0424 UT, and 237/0754 UT.

Broadfoot et al. [1989] suggested that plasma from Triton may be densest at the two longitudes where Triton's orbit intersects the magnetic equator. The predicted locations of these

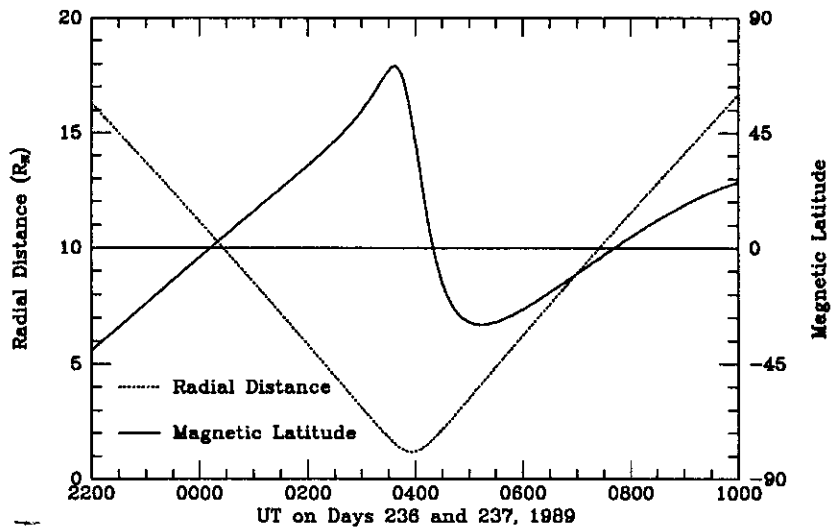


Fig. 1*b*. The radial distance and magnetic latitude of the spacecraft versus time.

hypothesized plasma arcs are shown by the shaded regions in Figure 1*a*; one arc is centered at 350° longitude (shown on the right side of the figure), and the other at 170° longitude (left side of figure). According to Figure 1*a*, the spacecraft seems to have crossed both plasma arcs, but since between 237/0300 UT and 237/0400 UT its position in magnetic coordinates is not certain, the plasma arc near 170° longitude may not have been crossed by the spacecraft. Even if the arc was crossed, the time that the spacecraft spent in it should be short, and no significant amount of particle flux would be detected because the location is at high magnetic latitudes and close to the planet, where loss cone effects may be important. It should be noted that although strong theoretical arguments predict the formation of these arcs, the PLS data do not confirm or refute their existence because of the limited nature of the sampling in magnetic longitude.

RESULTS

Overview of the Data

Plate 1, an energy-time color spectrogram of the electron current per energy channel, shows a complete and qualitative overview of the PLS electron data acquired during the Voyager encounter. It covers three time sequences: the top panel covers the time period from 236/1400 UT to 236/2000 UT (6 hours) when the spacecraft was in the inbound magnetosheath and subsolar cusp region [*Belcher et al.*, 1989], the middle panel covers the time period from 236/2200 UT to 237/1000 UT (12 hours) when the spacecraft was in the magnetosphere, and the bottom panel covers the time period 238/0600 UT to 240/0000 UT (42 hours) when the spacecraft crossed the outbound magnetosheath. Each panel contains two energy modes, E2 (channels 5 to 14, or energy from 140 eV to 3324 eV; higher channels are contaminated with noise and are not shown) on the top and E1 (channels 1 to 16, or energy from 10 eV to 140 eV) on the bottom. The color scale at the bottom of the plate indicates the values of the current in femtoamperes. Note that in the top and bottom panels the large (compared to the noise background) electron currents which steadily appear in the highest few channels of the E2 spectra are due to instrumental interferences and should be ignored.

Significant electron signals begin at the inbound bow shock crossing (BS) which occurred at 236/1428 UT and 34.8 R_N from Neptune. At this point, the cold solar wind electrons slowed down and heated up sufficiently to be observed above the 10-eV threshold of the instrument. The inbound magnetosheath was traversed by the spacecraft from 236/1438 UT to 236/1800 UT as indicated by the considerable currents of hot electrons. A typical spectrum from the inbound magnetosheath is shown in Figure 2*a*, where we plot the reduced distribution function [*Sittler*, 1983] versus energy. The spectrum is well characterized by a single Maxwellian with a temperature near 25 eV. The magnetopause (MP) crossing at 236/1800 UT is not sharp compared to magnetopause crossings seen by Voyager at the other planets, because the spacecraft entered the magnetosphere through the southern polar cusp region. Electron fluxes gradually decrease across the cusp region; electron spectra in the cusp region look similar to the spectrum shown in Figure 2*a*, but with reduced densities and temperatures.

Inside the magnetosphere of Neptune the PLS instrument observed four electron flux enhancements, three of which (those between 236/2320 UT and 237/0035 UT, at 237/0420 UT, and between 237/0640 UT and 237/0840 UT) occurred at low magnetic latitudes (see Figure 1*b*) and were tentatively called plasma sheet crossings [*Belcher et al.*, 1989]. But this interpretation is not unique. The two outer plasma enhancements, between 236/2320 UT and 237/0035 UT and between 237/0640 UT and 237/0840 UT, could also be the plasma arc which is predicted to be near 350° longitude (see Figure 1*a*). These two enhancements have similar features: the maximum flux of high-energy electrons (E2) appears farther away from Neptune than that of the low-energy electrons (E1), and at 237/0035 UT inbound and 237/0645 UT outbound, at approximately the same radial distance (8.5 R_N), electron fluxes drop below the threshold of the instrument. (The ion data, however, do not exhibit dramatic changes at these times.) The inner plasma sheet, crossed at about 237/0420 UT, after closest approach, is very close to the planet and is composed of hot plasma. It is followed by a short interval in which electron signals are absent, which will be ascribed in a subsequent section to ring absorption. After the ring absorption region, electron fluxes regain their former intensity at 237/0435 UT; this enhancement is probably the continuation of the inner plasma sheet. Throughout the inner magnetosphere, except in the hot inner plasma sheet, electrons have a cold bulk distribution with a temperature of a few electron volts and a high-energy tail which can be modeled using one or two hot Maxwellian distributions. Figure 2*b* shows an example of this type of spectrum.

In the magnetotail lobe (from ~237/0900 UT to 238/0819 UT), plasma signals are very low. The spectrogram in Plate 1 does not cover this period. The outbound magnetopause crossing occurred at 328/0819 UT, at which point significant electron currents appear in the low-energy channels. From 238/0819 UT to 239/2027 UT, more than two Neptunian days, the spacecraft stayed in the outbound magnetosheath. Most of the electron spectra are cold, like the one shown in Figure 2*c*. The electron temperature is only a few electron volts, while the spacecraft is charged to a positive potential greater than 10 V, thus making it difficult to analyze the data correctly. Electron parameters for the outbound magnetosheath are therefore not presented in this paper.

Inbound Magnetosheath and Cusp Region

Figure 3 shows the electron density (n_e), electron temperature (T_e) and spacecraft potential (Φ_{SC}) for the inbound magnetosheath and cusp region. Data from both E-short and E-long measurement modes are used in this plot. The empirical return current relation described by *Scudder et al.* [1981] was used to determine the spacecraft potential, which was a few volts positive.

Before the inbound bow shock crossing (BS), no electron signals were detected by the PLS instrument, but the solar wind proton density is accurately determined using the PLS ion data. For 2 hours before the shock crossing, the solar wind density, temperature, and velocity remained at an almost constant level of about 0.0045 cm^{-3}, 0.5 eV, and 400 km s^{-1}, respectively. Upon crossing the bow shock (236/1438 UT), the electron temperature rises to 13 eV, and the density to 0.017 cm^{-3}. The density increase is consistent with the jump condition for a strong shock. From 236/1438 UT to 236/1445 UT, when strong broadband waves were detected by the plasma wave subsystem (PWS) [*Gurnett et al.*, 1989; *Moses et al.*, 1990], the electron temperature continued to increase to a maximum value of 40 eV, while the electron density increased to 0.028 cm^{-3}. As the spacecraft moved toward the magnetopause, the electron density

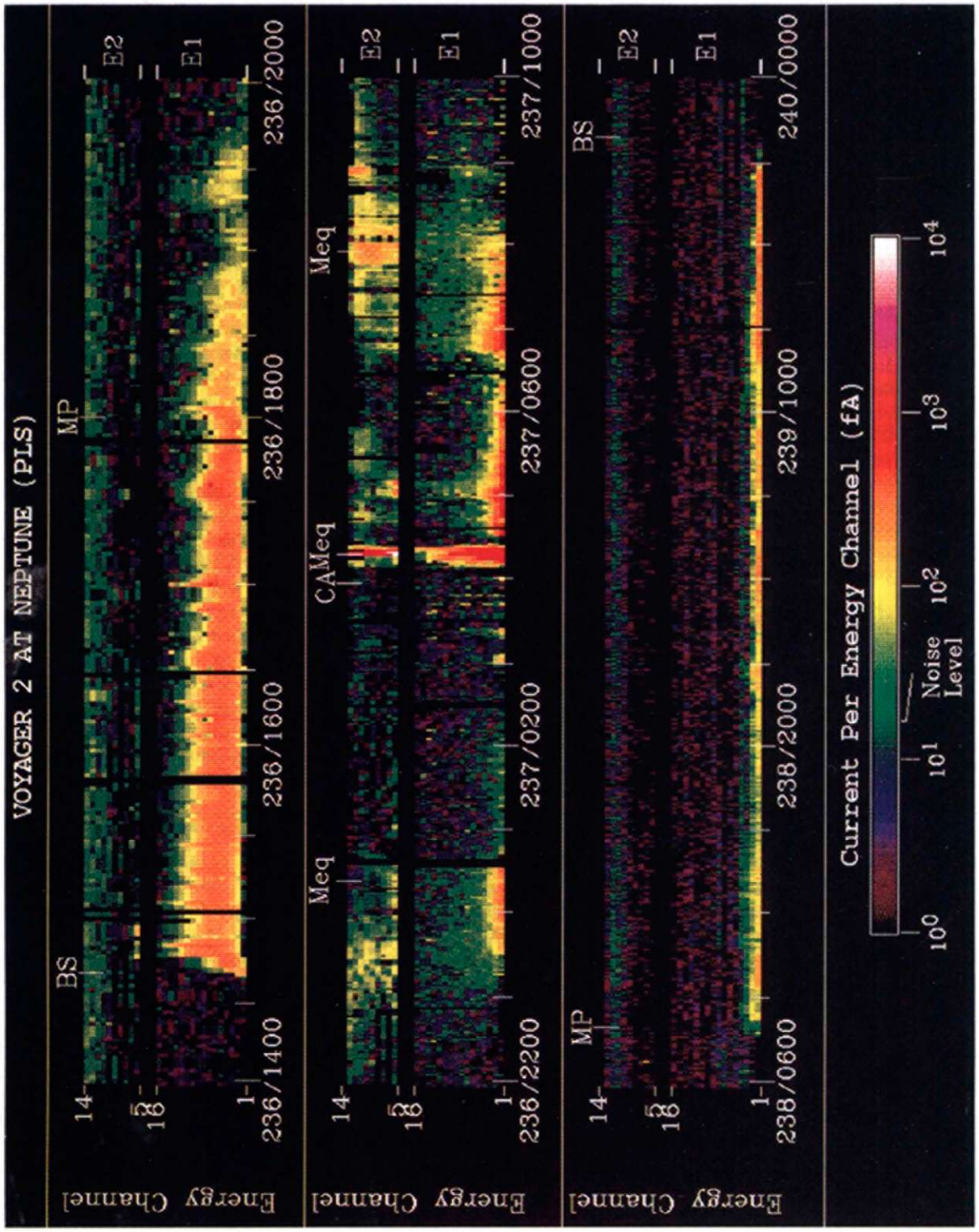


Plate 1. Energy-time color spectrograms of the PLS electron currents during the Neptune encounter. The horizontal color scale gives the color code of the current levels. The electron currents are related to the electron fluxes, except that they are a convolution of the instrument response function and particle flux (see *Sittler* [1983] for details).

in the magnetosheath gradually increased, which is consistent with the gasdynamic model of *Spreiter and Stahara* [1980]. The electron temperature, however, is not consistent with the gasdynamic model; it decreases toward the magnetopause.

The magnetopause crossing (MP), which occurred at 1800 UT [*Belcher et al.*, 1989; *Ness et al.*, 1989; *Szabo et al.*, 1991], is not associated with a distinct feature in the electron density, although the electron temperature does increase at this time. The electron density began to decrease more than 10 min before the magnetopause crossing. This is probably due to leakage of magnetosheath plasma across the boundary into the polar cusp. Inside the cusp region the electron density shows a general decrease, and the electron temperature is more or less correlated with the density variation; this could be evidence that the spacecraft encountered the plasma mantle [*Szabo et al.*, this issue].

Inner Magnetosphere

Electron density and temperature. Figure 4 shows the electron density and temperature with formal 1σ error bars [*Bevington*, 1969] for the time period from 236/2200 UT to 237/1000 UT. The spacecraft acquired a small negative charge in Neptune's magnetosphere as it did in some regions of the magnetospheres of Jupiter [*Sittler and Strobel*, 1987], Saturn [*Richardson and Sittler*, 1990], and Uranus [*Sittler et al.*, 1987]. Thus direct fits to the electron spectra do not give good estimates of the density in cold plasma regions. Most of the density points shown in Figure 4 are taken from the PLS ion data [*Richardson et al.*, this issue] because the ion measurements are less affected by the spacecraft potential because of their convective motion. The electron temperature of an individual Maxwellian component is calculated from the electron spectra; this value is reliable since the spacecraft charge has little effect on this calculation when the spacecraft is charged to a negative potential [*Sittler*, 1983]. The temperature

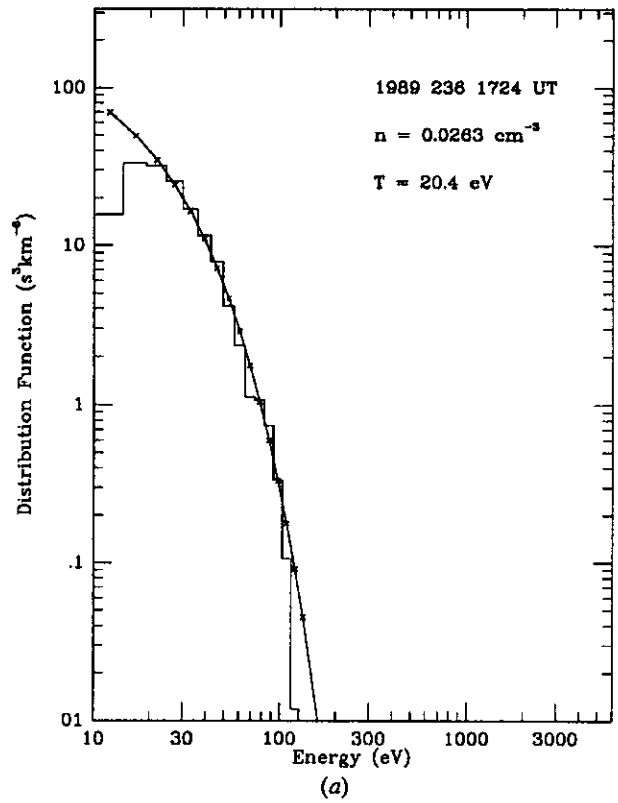


Fig. 2. Examples of electron spectra and their Maxwellian fits in the (*a*) inbound magnetosheath, (*b*) magnetosphere, and (*c*) outbound magnetosheath. Zero spacecraft potential is assumed in fitting the spectra.

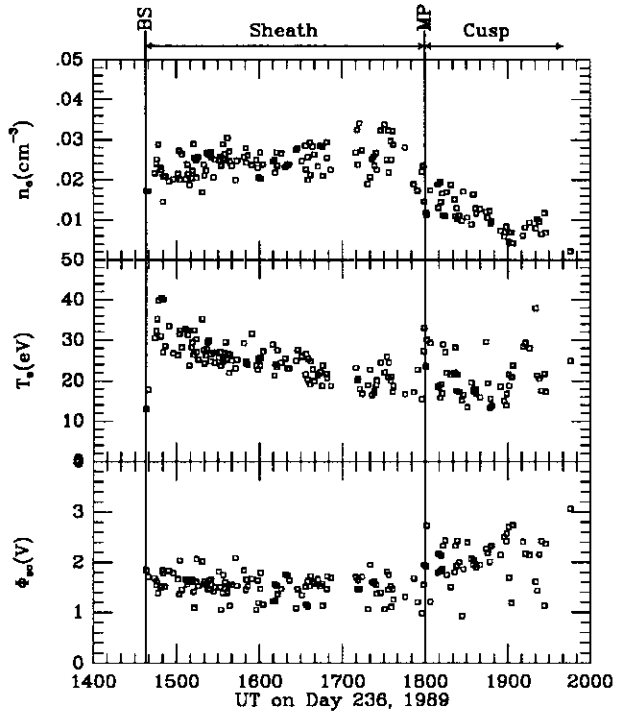


Fig. 3. The electron number density (n_e) and temperature (T_e) and the spacecraft potential (Φ_{SC}) in the inbound magnetosheath and polar cusp region.

shown in Figure 4 is the average of the temperatures of several Maxwellians weighted by their true density. (Here the true density of a Maxwellian means that it has been corrected from the effect of spacecraft charging so that the sum of all components is equal to the total ion density.) This value therefore depends on the ion density, so the errors from the ion density calculation together with those from the electron fits contribute to the error bars of the electron temperature in Figure 4.

Inbound, electrons are first detected in the inner magnetosphere at 236/2245 UT and have a density of 2.5×10^{-3} cm^{-3}. This is 50 min earlier than the first detection of ions at 236/2335 UT. The electron temperature is 50–200 eV, which is much greater than the spacecraft potential. Therefore densities calculated from electron spectra should be accurate in this time period. The results are shown by the solid circles in Figure 4. Starting at 236/2337 UT, the electron spectra contain a cold component. Since the temperature of this cold component is comparable to the spacecraft potential, densities derived from these electron spectra are seriously affected by the spacecraft charge. Thus ion data provide the only reliable density estimates in this region; they are plotted in Figure 4 using open circles. From 236/2337 UT to 237/0035 UT the density increases from 0.01 cm^{-3} to 0.1 cm^{-3} and the electron temperature decreases from 25 eV to 7 eV. At 237/0045 UT (237/0035–237/0045 UT is a data gap) the cold electron component suddenly disappears, and only a minor hot electron component is seen in the spectra. The electron density derived from the fits has a clear discontinuity at this time, but the ion density does not show any change. If this were caused by a sudden change of the spacecraft potential, a large negative spacecraft potential would be required to satisfy charge neutrality. But the PLS ion measurements do not show any evidence of a large negative spacecraft potential at this time. A possible explanation is that the thermal electrons cool below approximately 3 eV, the temperature below which electrons with a density of the order of 10^{-2} cm^{-3} would not be detected by the PLS instrument. The electron spectra between 237/0045 UT and 237/0242 UT contain only hot electron components, which have total densities much less than the total ion density of 0.02 cm^{-3} to 0.1 cm^{-3}. Because the cold electron component is completely missing, no information is available about its temperature. To estimate the total electron temperature we use the upper limit of 3 eV for the cold component; the density of cold electrons is the total electron density (derived from the ion density) minus the hot electron density. The electron temperature shown in Figure 4 for this time period is the weighted average of these 3-eV cold electrons and the hot electrons and is thus an upper limit for the temperature. After 237/0242 UT the electron measurements show only background noise until closest approach. Although ions are observed near 237/0300 UT, the electron spectra at this time cannot be analyzed, and the electron temperature is unknown.

The plasma detected by the PLS instrument near 237/0420 UT, close to the planet and near the magnetic equator crossing, is hot and relatively dense. The maximum electron density and temperature are 2 cm^{-3} and 90 eV, respectively. This is followed by a low plasma density region starting at 237/0427 UT which we ascribe to ring absorption (see below). The density in this time period (from the ion data) is about 3×10^{-2} cm^{-3}, but the electron temperature cannot be determined. After 237/0435 UT the electrons become cold again. The variation of electron parameters outbound is very similar to that observed during the inbound leg.

Cold and hot electrons. Since the spectra of the electrons in the magnetosphere are not well described by a single Maxwellian, the total electron density and temperature do not provide complete information about the electron distribution function. Most of the spectra in Neptune's magnetosphere can be simulated using a cold Maxwellian component and several hot Maxwellian components, as shown in Figure 2*b*. Figure 5 shows the temperature of the cold electrons (T_c) from 236/2200 UT to 237/1000 UT. Like the total electron temperature, T_c decreases toward closest approach. The true density of the cold electron component is not shown because it is almost the same as the total electron density shown in Figure 4; instead, we show in Figure 6 the cold electron density obtained by fitting the electron spectra with the assumption of zero spacecraft potential. This density is a factor of 2-10 lower than the ion density obtained in the same time period, and this discrepancy is used to determine the spacecraft potential.

Electrons with temperatures above 15 eV are called hot electrons in this paper. Figure 7 shows the ratio of the hot electron density to the total electron density (n_h/n_e) (top panel) and the temperature of hot electrons (T_h) (bottom panel). In the three hot plasma regions the ratio n_h/n_e is 1. In the time periods when the cold electrons are present, hot electrons are a small fraction of the total population; the ratio n_h/n_e is usually a few percent. The hot electron temperature in Figure 7 is calculated by using one or two hot Maxwellian distributions to fit the data, and then taking a weighted average of the temperatures. For most of this time period the hot electron temperature is 100-200 eV. These hot electrons make a considerable contribution to the ionization rate of neutral atoms in the Triton's torus despite their low density, since the ionization rates of hydrogen and nitrogen peak at T_e~300 eV.

Spacecraft charging. Previously, we mentioned that the spacecraft had a small negative charge in the magnetosphere.

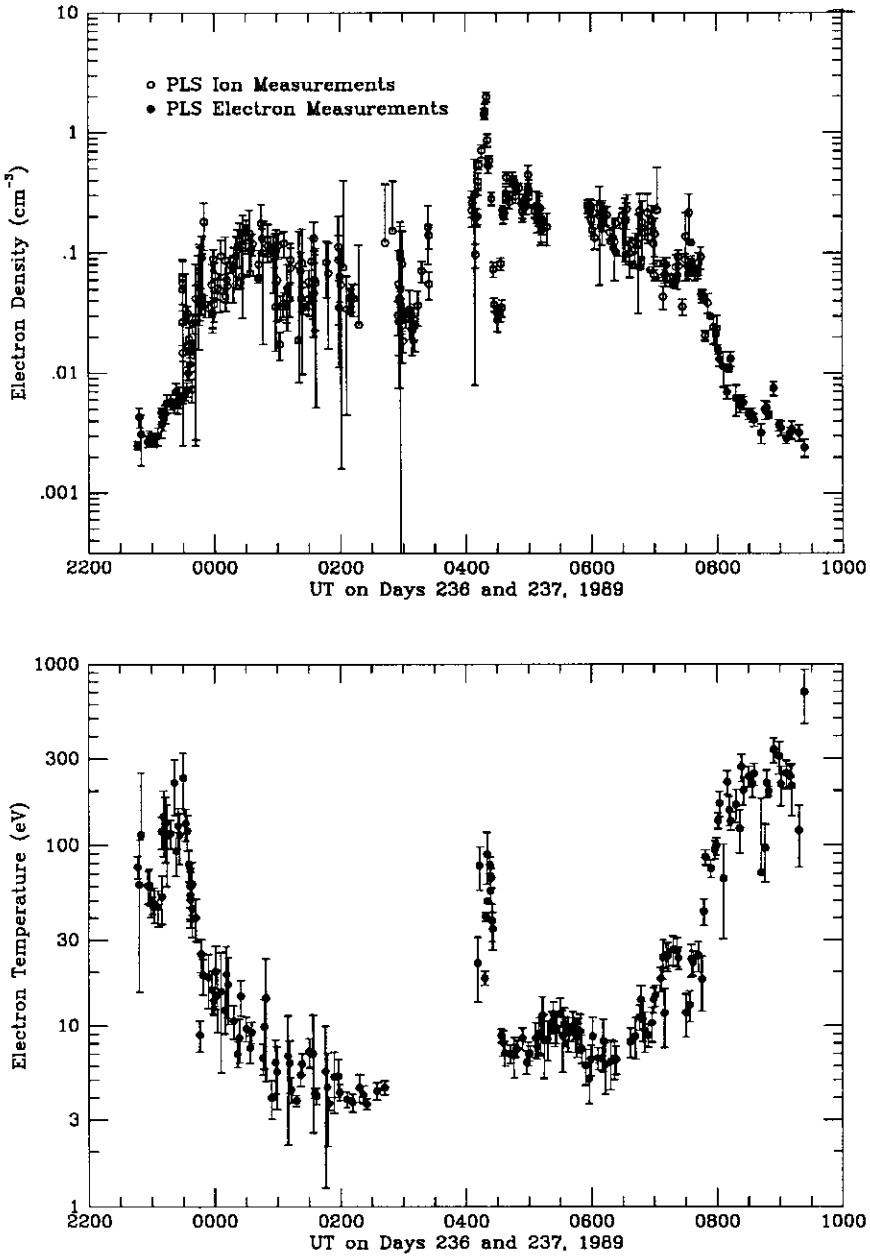


Fig. 4. Electron number densities (top) and total electron temperatures (bottom) for the time period from 236/2200 UT (day/hour minute) to 237/1000 UT, during which Voyager was in the magnetosphere of Neptune. The error bars are 1σ deviations.

The total density obtained from fits to the electron spectra is less than the ion density obtained by *Richardson et al.* [this issue]. We use the condition of charge neutrality to determine the spacecraft potential when the cold electron density is available from the fits. To first approximation the spacecraft potential (Φ_{SC}) is

$$\Phi_{SC} = \frac{kT_c}{e} \ln\left(\frac{n_c}{n_t - n_h}\right) \quad (1)$$

where k is Boltzmann's constant, e is the unit electric charge, T_c is the cold electron temperature, n_c is the cold electron density from the spectral fits with $\Phi_{SC} = 0$, n_t is the total electron density, which is set equal to the ion density, and n_h is the hot electron density. Ion and electron measurements are not taken simultaneously, and in order to get the total electron density at the times when the electron measurements were taken, we linearly interpolate the ion data. The hot electron density n_h is taken directly from the fits to the electron spectra as it is not affected by a small spacecraft charge.

Figure 8 shows the results of the calculation of the spacecraft potential Φ_{SC}. Also shown are 1σ error bars [*Bevington*, 1969], due mostly to the uncertainties of the ion densities n_t, cold electron densities n_c, and cold electron temperatures T_c. As expected, the spacecraft potential is generally small, less than 20 V negative.

This result is consistent with that derived independently from the ion measurements. *Richardson et al.* [this issue] fit all the ion spectra in the plasma sheet crossings near 237/0000 UT and 237/0700 UT. They found that ions generally appear to be

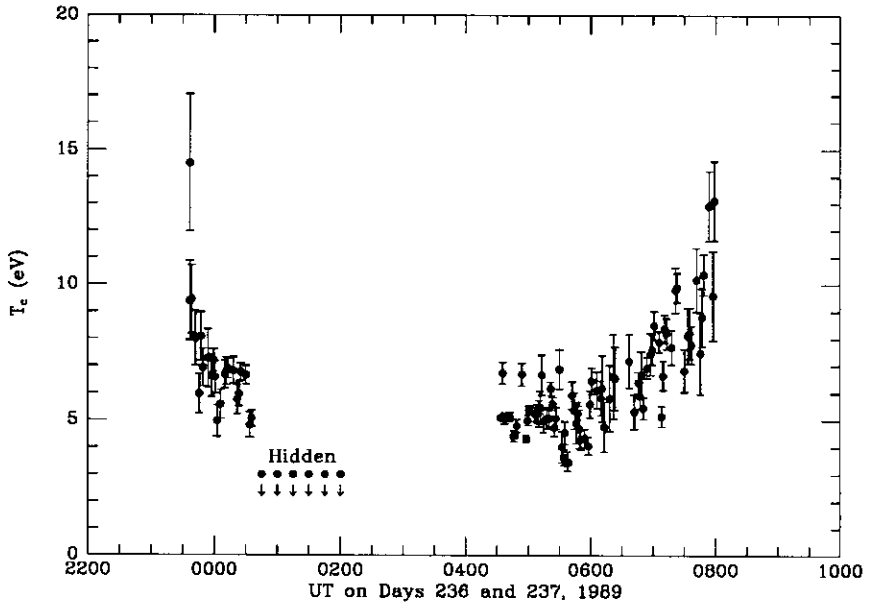


Fig. 5. The temperature of the cold electron component (T_c) in the magnetosphere of Neptune. The data points labeled "hidden" are the upper limit for the cold electron temperature when the electron fluxes are below the instrument threshold.

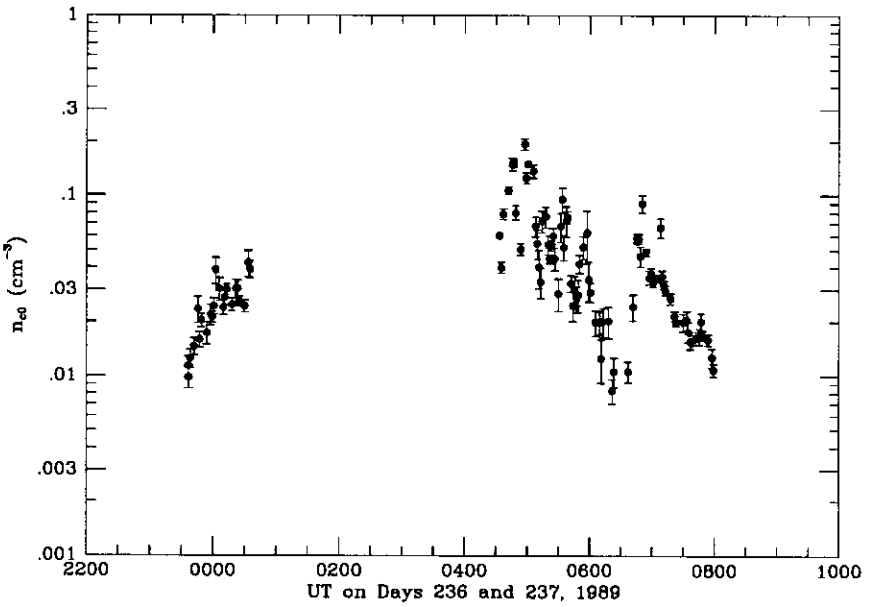


Fig. 6. The cold electron number density (n_c) in the magnetosphere of Neptune derived from Maxwellian fits to the data assuming zero spacecraft potential. The density is much smaller than the total plasma density, indicating that the spacecraft is negatively charged.

supercorotational in these regions. But the plasma beta value is small in Neptune's magnetosphere [*Krimigis et al.*, 1990], and the corotation speed dominates the convection speed at Neptune [*Selesnick*, 1990]; thus departure from rigid corotation is not expected. The most plausible explanation of the apparent supercorotation is that the spacecraft had a negative charge, which accelerated positive ions into the PLS detectors. The spacecraft potential corresponds to the difference between the apparent plasma flow energy of the ions and the corotational energy. The potentials derived from a few high-resolution ion spectra are plotted in Figure 8 using stars. The error bars for these points are not determined but are probably large. Within the expected uncertainties these data points agree reasonably well with the results obtained here, particularly in the outbound time period.

DISCUSSION

Plasma Sources and Sinks

To locate sources and sinks of plasma, we plot in Figures 9 and 10 the plasma density and temperature versus the spacecraft L shell calculated using the I8E1 magnetic field model. Within error bars (see the previous section), these figures show an

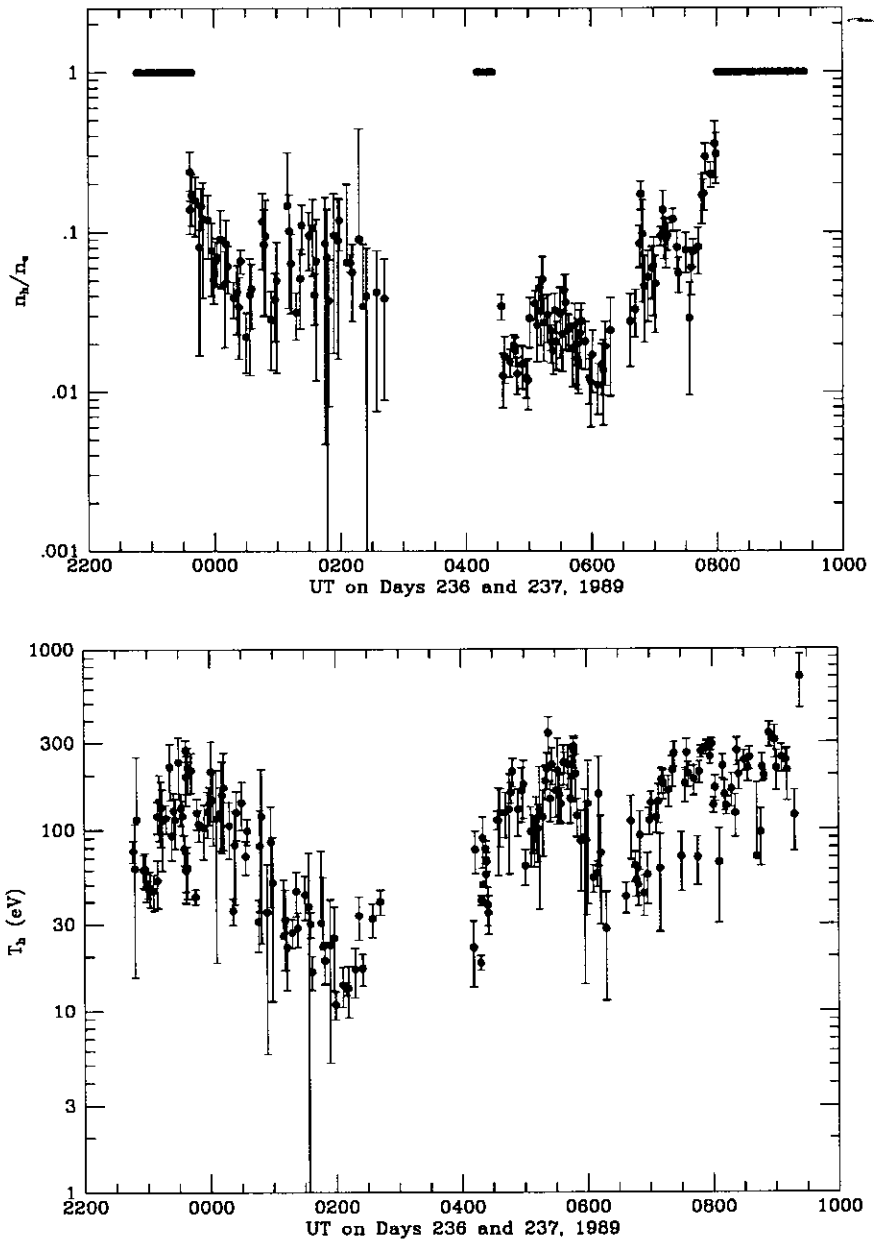


Fig. 7. The ratio of hot electron density to total electron density n_h/n_e (top) and the temperature of hot electrons T_h (bottom) in the magnetosphere of Neptune.

inbound-outbound symmetry outside L=8.5. The spacecraft remained at large L shells and high latitudes during most of the inbound pass, so no inbound data were obtained inside L=8. Between L=8 and L=8.5, the inbound data points are slightly below those obtained outbound, but the error bars for the electron density and temperature in this region are relatively large, as described in the previous section. Except at the smallest L shells, the electron density in Figure 9 shows an overall decrease as the L shell increases. The electron temperature remains roughly constant between L=2 and L=8.5; beyond L=8.5 the temperatures increase rapidly until about L=14. We suggest in a later subsection that the boundary at L=8.5 is the inner edge of Triton's neutral torus.

Knowledge of the plasma flux tube content (N), the total number of particles per unit L shell for a given species, is necessary to understand diffusive and convective transport of the plasma since the quantity NL^2 is conserved by these processes. Calculation of N requires as input the density and temperature of each electron and ion component. This calculation was performed by *Richardson et al.* [this issue]. Instead of repeating these computations here, we make the following estimate to show that NL^2 is proportional to the plasma density times L^4. We assume that all the plasma species are isotropic in velocity space, uniformly distributed in longitude, and isothermal along a given magnetic field line. In the region where the centrifugal force is dominant, the ion scale height is [*Hill and Michel*, 1976]

$$H_c = \frac{1}{\sqrt{3}\,\pi}\, v_{th}\, T \tag{2}$$

where T is the rotation period of the planet and v_{th} is the

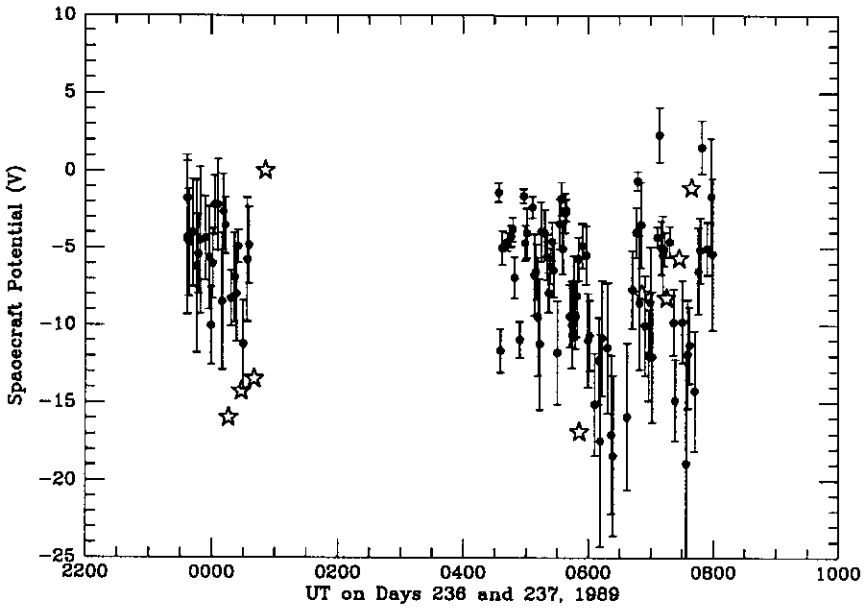


Fig. 8. The electric potential of Voyager 2 in the magnetosphere of Neptune.

thermal speed of the ion. In Neptune's magnetosphere the typical thermal speed is 30 km s^{-1} for protons and 20 km s^{-1} for N^+. The scale height is then 13 R_N for protons and 8.6 R_N for N^+. To maintain charge neutrality, the scale height of the electrons must be between these two numbers, depending upon the density ratio of protons to N^+. The most probable electron scale height is 11 R_N. This value is comparable with or bigger than the L shell values at which the plasma was detected by the spacecraft. Furthermore, the gravitational force acting on particles is important close to the planet. The direction of the gravitational force is opposite to the centrifugal force, thus making the scale height even larger. The large scale height means that the electron and ion densities are almost uniform along magnetic field lines. The flux tube content N is the product of the density times the flux shell volume, the total volume per unit L shell. In a dipole magnetic field, the flux shell volume is proportional to L^2. In fact, the magnetic field of Neptune is more complicated than a dipole field; the I8E1 magnetic field model was used in this calculation. However, the flux shell volume still roughly follows the L^2 law. The quantity NL^2 is then proportional to nL^4. Since NL^2 is conserved during diffusive and convective transport, it remains constant in the absence of plasma sources and losses. In this limit the electron density should be proportional to L^{-4}. The smooth dashed curve in Figure 9 shows this relation. This curve is not a fit to the data, but shows a baseline for the density variation in this limit. In making the curve, we took the electron density at L=14.3 as the initial point.

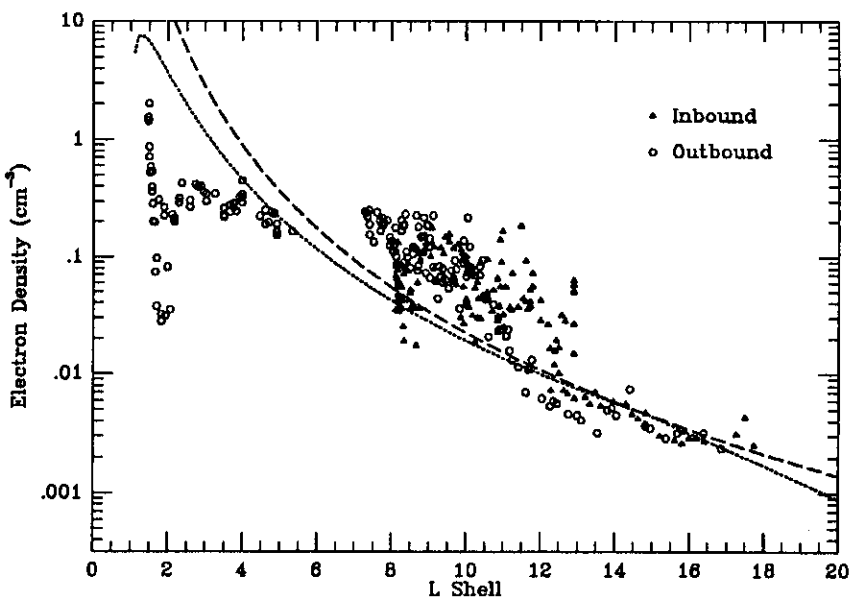


Fig. 9. The electron density versus the I8E1 L shell. The open circles are outbound data, and triangles are inbound data. The dashed line shows the expected density variation for a constant flux shell content model, and the dotted line shows densities derived using a diffusion model.

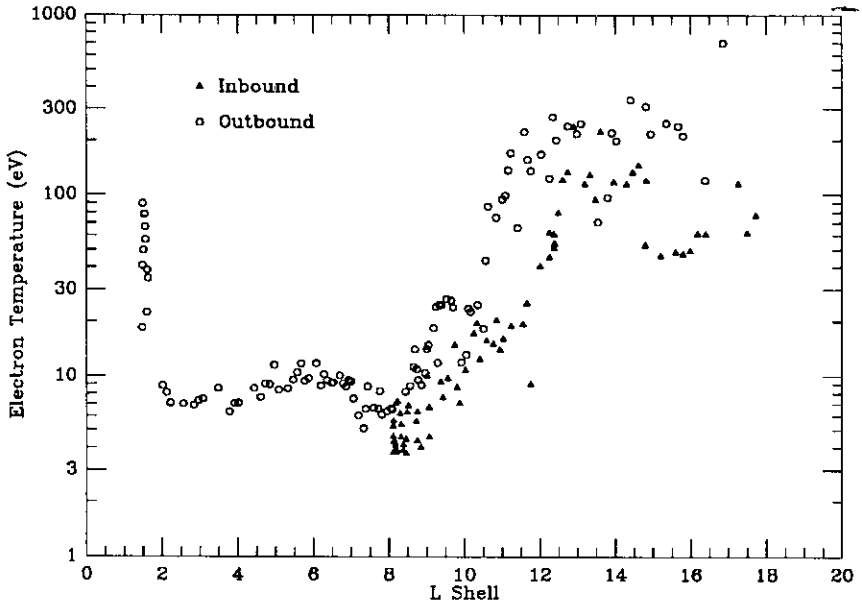


Fig. 10. The total electron temperature versus the I8E1 L shell.

However, in reality, the magnetosphere of Neptune is neither source-free nor loss-free. The most important plasma source is Triton, which injects charged particles as well as neutral atoms into the magnetosphere at a rate of 10^{25} s^{-1} [*Broadfoot et al.*, 1989; *Yung and Lyons*, 1990]. Assuming steady state, the plasma must be removed from the magnetosphere at the same rate they are added. We assume that the plasma has a point source at Triton and sinks at the surface of the planet and the magnetopause. We further assume that the plasma density is longitudinally symmetric although strong theoretical arguments dispute this [*Broadfoot et al.*, 1989; *Richardson et al.*, 1990, *Selesnick*, 1990]. For diffusion with a diffusion coefficient of the form $D_{LL} = D_0 L^3$ [*Coroniti*, 1974], where D_0 is a constant, the steady state density profile is given by [*Siscoe*, 1979]

$$n = \frac{F_i}{4\pi\theta_c R_N^3 D_0} \frac{\ln L}{L^4} \quad \text{for } L < L_r \tag{3}$$

$$n = \frac{F_o}{4\pi\theta_c R_N^3 D_0} \frac{\ln (L_b/L)}{L_r L^3} \quad \text{for } L > L_r \tag{4}$$

where L_r is the L shell of the satellite source, L_b is the outer boundary of the magnetosphere, $L=1$ is the inner boundary, and θ_c is the half-cone angle of the magnetospheric plasma cloud viewed from the planet. The quantities F_i and F_o are inward and outward fluxes of plasma which have the ratio $F_i/F_o = \ln(L_b/L_r)/\ln L_r$. In this case, $L_r = 14.3$, $L_b = 26$, and $\theta_c \sim 1$. The total of F_i and F_o is the particle flux from Triton (10^{25} s^{-1}), and their ratio is ~0.22; thus the inward and outward fluxes F_i and F_o are 2×10^{24} s^{-1} and 8×10^{24} s^{-1}. Fitting the theoretical curve to the electron density at $L=14.3$, we find that D_0 is 1×10^{-7} R_N^2 s^{-1}. This number is consistent with *Richardson et al.* [this issue]. It implies that plasma transport in the magnetosphere of Neptune is very fast compared to that of Jupiter and Saturn. The mechanism driving this fast plasma transport is not understood.

The dotted line in Figure 9 shows the theoretical density profile derived from the diffusion model, which is very similar to the profile obtained using the assumption of constant NL^2. Comparing the electron density with the model curves, we find that the actual density is higher than the theoretical value in the region from $L=8$ to $L=12$. This region must contain a local plasma source. If we raise the curves to fit the data at $L=10$, we find the plasma density beyond $L=12$ is below the curves; plasma loss must occur in this case. At this time we can think of no plasma loss mechanism at these L shells. Thus we suggest that there is a plasma source between $L=8$ and $L=12$ resulting from local ionization of neutral hydrogen atoms escaping from Triton. *Richardson et al.* [this issue] also deduce from the temperature profile of protons that a proton source exists in this region. In the next subsection we show that the ionization rate in this region is higher than in the adjacent regions. The electron temperature profile in Figure 10 shows a rapid decrease from $L=12$ to $L=8$, which indicates cooling.

Inside $L\sim5$, the electron density is lower than the theoretical curves predict, indicating that substantial plasma losses occur near Neptune. Possible loss mechanisms are small-satellite and ring absorption, precipitation into the atmosphere of Neptune, and charge exchange with Neptune's neutral hydrogen corona. The last mechanism is discussed in detail by *Richardson et al.* [this issue]. Here we will discuss the first two mechanisms.

Ring absorption and satellite sweeping of charged particles were observed during many previous planetary encounters [e.g., *Van Allen et al.*, 1980; *Simpson et al*, 1980; *Sittler et al.*, 1981; *Van Allen*, 1983; *Krimigis and Armstrong*, 1982; *Lazarus et al.*, 1983, *Sittler et al.*, 1983], but most of these signatures were detected in the high-energy particles. In the case of Neptune's magnetosphere, plasma transport is very fast; the absorption of low-energy charged particles by satellites is very difficult to detect because the total absorption cross section of the satellites is much smaller than that of the rings and because the satellite absorption occurs over a very small range of L shells. Ring absorption of low-energy particles is easier to observe because the loss region covers a larger area. These signatures are observed only when the spacecraft and the ring are on the same magnetic field line. The detailed behavior of ring absorption depends upon the properties of the particles or dust that constitute the ring.

Figure 11 shows electron and ion currents measured by the PLS experiment. The solid line is the electron current in the D cup, the dotted line is the ion current in the D cup, and the dashed line is the ion current in the C cup. The three smooth curves show the variation of the radial distance (R_{eq}) of the ring plane intersection point of the magnetic field line that passes through the spacecraft. Three different magnetic field models, the OTD model, the I8E1 field model with all terms, and the I8E1 field model with only the resolved terms, were used in the calculations. All models agree with each other quite well, implying that the calculation of R_{eq} is not sensitive to the field model chosen. When the distance R_{eq} is equal to the radius of a ring, the spacecraft is magnetically connected with that ring. The three horizontal lines labeled with 1989N1R, 1989N2R, and 1989N3R indicate the locations of Neptune's three rings. A sheet of ring material (see Figure 17 by *Smith et al.* [1989]) extends from radius ~1.65 R_N to ~2.38 R_N, as indicated by the shaded stripe. Fluxes detected by the PLS instrument are lower in this region than in the surrounding regions. Since this feature is correlated with the location of the broad ring, we tentatively attribute this decrease to ring absorption. The ring 1989N1R does not produce such a feature, perhaps because it is so narrow.

Mauk et al. [1990] report a feature in the low-energy charged particle (LECP) data which they claim is due to ring absorption. But this feature was observed at 237/0419 UT, 8 min earlier than the minimum in the PLS data. This difference is not understood. The cosmic ray (CRS) data show a dip in flux from 237/0428 UT to 237/0442 UT [*Stone et al.*, 1989], which is at roughly the same time as the one in the PLS data. This decrease in the CRS fluxes is interpreted as an absorption signature of a combination of small satellites and rings.

If the depletion in the fluxes near 237/0430 UT is due to ring absorption, we can estimate limits for the plasma transport time. The radial diffusion must be slow enough so that when the diffusion balances ring absorption losses, a significant feature is present in the data. We assume that the radii of ring particles are much smaller than the gyroradius of charged particles (~1 m). Then the time scale for the ring absorption τ_a is

$$\tau_a = \frac{\tau_B \cos\beta}{2\,\xi\,\tan\alpha_0} \tag{5}$$

where τ_B is the bounce time, ξ is the optical depth, α_0 is the average particle pitch angle, and β is the angle between the magnetic field lines and the normal to the ring plane. The bounce time τ_B is estimated to be 10^2 s for protons with kinetic energies of the order of 100 eV (here we use the ion bounce time rather than the electron bounce time, because ions limit the electron loss rate to maintain charge neutrality, and the ion absorption cross section is less affected by the charge of ring material and closer to the optical absorption cross section). The optical depth ξ is 10^{-4} [*Smith et al.*, 1989]. The quantity $\cos\beta/\tan\alpha_0$ is of the order of 10^{-1} if the proton anisotropy $A \equiv T_\perp/T_{||} = 11$ as determined by *Richardson et al.* [this issue]. Therefore the ring absorption time τ_a is about 10^5 s. Thus 10^5 s is the lower limit for the radial diffusion time. To estimate an upper limit, we note that hot plasma was observed inside the ring system in the PLS data (see Plate 1 and Figure 11). Plasma of planetary origin would be cold (the ionospheric temperature is about 950°K [*Tyler et al.*, 1989]), so this plasma probably comes from outside the ring. One possible mechanism for transport across the ring is for low-energy particles to diffuse inward at longitudes where the ring is at high magnetic latitudes and spans a large range of L shells. At these longitudes only those ions and electrons with small pitch angles collide with the ring matter. The condition for this mechanism to be viable is that the time scale for the gradient drift be longer than the radial diffusion time. For 1-keV particles (the temperature of the N^+ ions near closest approach [*Richardson et al.*, this issue]) the drift time τ_{DB} at $L=2$ is 10^7 s. Thus the radial diffusion time for low-energy plasma at the location of the ring should satisfy 10^5 s $< \tau_d = D_{LL}^{-1} < 10^7$ s. Using the D_0 value of 1×10^{-7} R_N^2 s^{-1} we found previously, we can evaluate D_{LL}, finding that $D_{LL} = 8\times10^{-7}$ R_N^2 s^{-1} at $L=2$. Then the diffusion time is 1.25×10^6 s, which is consistent with the above condition.

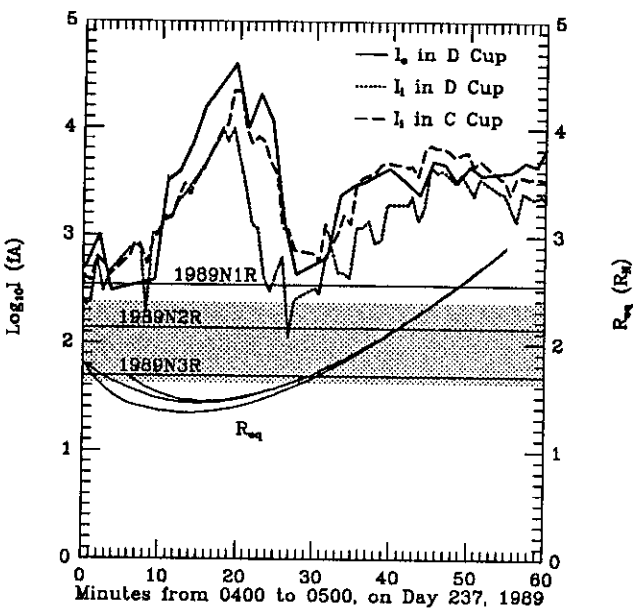


Fig. 11. The PLS electron and ion currents for the time period from 237/0400 UT to 237/0500 UT. The three smooth curves show the radial distance of the ring plane intersection point of the magnetic field lines that pass through the spacecraft, using three different magnetic field models. The three horizontal lines represent the positions of Neptune's three major rings. The depletion of the currents at about 0430 UT corresponds to crossing of the inner (broad) ring in the shaded region.

The absorption feature also allows us to calculate the diffusion coefficient quantitatively. The equation that governs the variation of the plasma density n in the absorption region is [*Fälthammar*, 1968]

$$L^2 \frac{d}{dL}\left[\frac{D_{LL}}{L^2}\frac{d}{dL}(nL^4)\right] = -\frac{nL^4}{\tau_a}\,. \tag{6}$$

Using dimensional analysis, we estimate the absorption width ΔL from equation (6) and find that $\Delta L = (\tau_a D_0 \bar{L}^3)^{1/2}$. Taking $\Delta L = 0.3$ and $\bar{L} = 2$ from Figure 11, we find that $D_0 = 1.1\times10^{-7}$ s^{-1}. This is again consistent with the previous result.

In addition to absorption by particulates, another plasma loss mechanism is particle precipitation into Neptune's atmosphere, which is particularly important when the spacecraft is close to the planet. The largest loss cone angle at the spacecraft position, calculated using the I8E1 magnetic field model, is about 40° and occurred near closest approach. The distribution function will have few particles with pitch angles within the loss cone, so the PLS instrument will detect an "anisotropic" spectrum. Strong

evidence for this effect is reported by *Richardson et al.* [this issue], who fit a set of ion spectra using a bi-Maxwellian distribution function and found a large anisotropy ($A \equiv T_\perp/T_{||}$), 11 for H^+ and 3 for N^+. We compare electron and ion fit parameters in the hot plasma region near 237/0420 UT. Electron densities obtained from fits using Maxwellian distributions and the assumption of zero spacecraft potential are an order of magnitude lower than the ion densities. Large spacecraft potentials of 50 V to 130 V negative would be required to balance the electron and ion densities. But no evidence of such large spacecraft potentials is observed in the PLS data. (PLS would observe a beam of ions; see Figure 5 of *McNutt et al.* [1987].) As an alternative explanation, we note that the magnetic field data from the Voyager magnetometer experiment indicate that the D cup was looking roughly parallel to the magnetic field during this time period; the electron measurements should thus be strongly affected by a loss cone plasma distribution. Ion measurements, which are made in four different look directions, are less affected, since normals to the three main cups are perpendicular to the magnetic field lines. The result is that the density of ions obtained from the fits is larger than that of electrons because of the look direction of the PLS detectors in relation to the loss cone.

Triton Torus

As mentioned previously, the electron density and temperature data (Figures 9 and 10) contain signatures which we attribute to a Triton-generated neutral cloud or torus with an inner boundary at about 8 R_N. Using this boundary location and Equation (3) of *Cheng* [1990], which relates the inner boundary radius of the torus to the escape velocity of neutrals from Triton, we derive an ejection speed of ~0.6 km s^{-1} for the escaping atoms. The full thickness of the Triton neutral torus for this ejection speed is about 2 R_N [*Cheng*, 1990].

Hot electrons ionize the neutral atoms and create additional plasma locally in the torus. Along the spacecraft trajectory the ionization frequency ν_i of neutrals and ions can be calculated using the electron data. The ionization frequency is defined as

$$\nu_i = n_e \langle \sigma_i v \rangle = \int \sigma_i(v) v f_e(v)\, dv \tag{7}$$

where σ_i is the ionization cross section and $f_e(v)$ is the electron distribution function. Since the electron distribution can be represented as several Maxwellians, the ionization frequency ν_i is

$$\nu_i = \sum_M n_{eM} \langle \sigma_i v \rangle_{T_M} \tag{8}$$

where n_{eM} is the electron density of a Maxwellian distribution and $\langle \sigma_i v \rangle_{T_M}$ is the ionization rate for such a distribution, which is tabulated by *Lotz* [1967]. The results of this calculation are shown in Figure 12.

For neutral hydrogen the ionization frequency is of the order of 10^{-10} s^{-1} in the torus (some inbound data points near L=8 have large error bars because of the uncertainty in the electron temperature). It has a peak at L=10 and then decreases at larger L shells. The ionization frequency profiles for neutral nitrogen and singly ionized nitrogen have approximately the same shape, but at different values. The PLS instrument did not detect N^{++} in the magnetosphere; this is as expected since the ionization rate of N^+ is small and the density of N^+ is very low compared to the density of neutral atoms (see below). Photoionization rates, 2.1×10^{-10} s^{-1} for N and 8.1×10^{-11} s^{-1} for H [*Huebner and Giguere*, 1980], are comparable to the electron impact ionization rate, so photoionization is also an important source of plasma.

Although the lifetimes against ionization of neutrals (~10^9 s) are very long compared with the plasma transport time (~10^5 s), we still see significant amounts of plasma produced by local ionization. This means that the neutral cloud must be sufficiently dense for the particle production rate to balance the radial diffusion loss. In a steady state the equation governing this equilibrium is

$$\frac{dn}{dt} = N_n \nu_i - \frac{n}{\tau_D} = 0 \tag{9}$$

where N_n is the density of neutrals and τ_D is the diffusion time. Then the neutral density is of the order of 10^3 cm^{-3}. Most of these neutral atoms in the torus are probably hydrogen, because the thermal escape rate of hydrogen is ~10^{25} s^{-1}, which is much greater than the escape flux of neutral nitrogen [*Broadfoot et al.*, 1989].

This dense neutral hydrogen cloud is an electron energy sink due to atomic excitation and ionization. Newly created electrons have little kinetic energy initially; they need to gain an energy of $(3/2)T_e$ to reach thermal equilibrium with the ambient electrons. The electron energy equation may be written as

$$\frac{3}{2} n_e \frac{dT_e}{dt} = -\left[\frac{d\varepsilon}{dt}\right]_i - \left[\frac{d\varepsilon}{dt}\right]_{ex} + \left[\frac{d\varepsilon}{dt}\right]_{ie} - \nabla \cdot \mathbf{q}_e \tag{10}$$

where on the right-hand side the first term is the cooling due to ionization of neutrals (including the energy needed for the acceleration of newly picked-up electrons), the second term is the cooling due to atomic excitation, the third term is energy transfer from ions to electrons, and the last term is the divergence of the electron heat flux. If we only discuss the radial profile of electrons, the heat flux across magnetic lines can be neglected (we have ignored the possibility of ionospheric coupling for which electron heat flux can easily travel along field lines and deposit energy into the ionosphere where energy transport across field lines can occur). The rest of terms may be written explicitly as

$$\left[\frac{d\varepsilon}{dt}\right]_i = (\phi_i + \frac{3}{2}T_e) I_i N_n n_e \eta \tag{11}$$

$$\left[\frac{d\varepsilon}{dt}\right]_{ex} = N_n n_e \rho \eta \tag{12}$$

and

$$\left[\frac{d\varepsilon}{dt}\right]_{ie} = \nu_{ie} n_i n_e (T_i - T_e) \tag{13}$$

where $I_i = \langle \sigma_i v \rangle$ is the ionization rate, ϕ_i = 13.6 eV is the ionization potential, ρ is the atomic excitation cooling rate, η (~0.2) is the fraction of time spent by an electron in the neutral torus, and ν_{ie} is the Coulomb collision rate between ions and electrons. Since the neutral density is much bigger than the ion density, the third term in (10) can be dropped. The other two terms can both be important, depending on the electron

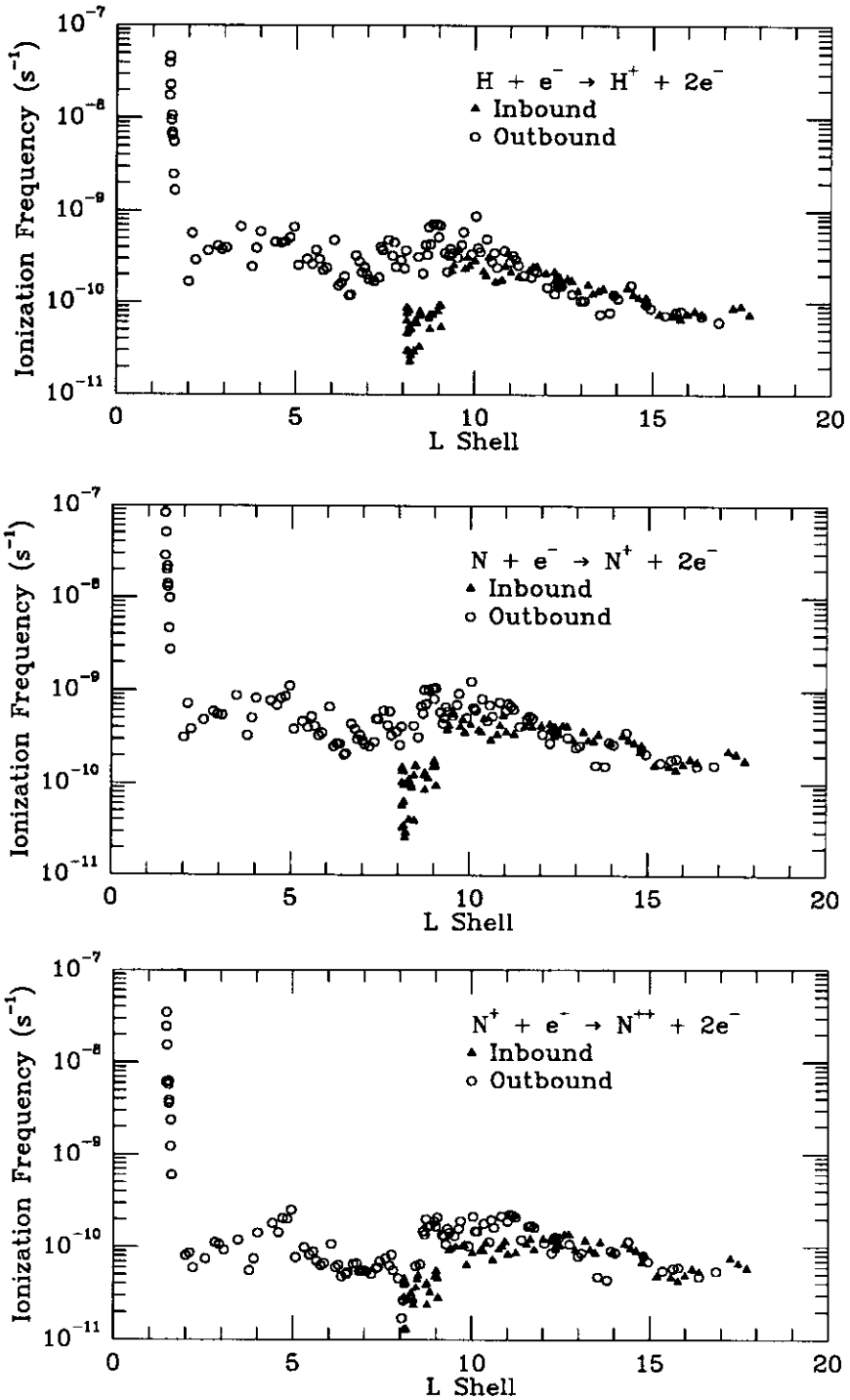


Fig. 12. Ionization frequencies for H (top), N (middle), and N^+ (bottom) along the spacecraft trajectory.

temperature. For example, if the electron temperature T_e = 10 eV, $(\phi_i+(3/2)T_e)I_i$ is 1.5×10^{-7} eV cm^3 s^{-1}, while ρ is 1.9×10^{-7} eV cm^3 s^{-1}. Combining (11) and (12), we rewrite (10) as

$$\frac{3}{2}\frac{dT_e}{dt} = -N_n \rho_{tot} \eta \tag{14}$$

where ρ_{tot} is $\rho + (\phi_i+(3/2)T_e)I_i$. For cold electrons ($T_e \sim 10$ eV), ρ_{tot} can be approximated as $\rho_0 T^\gamma$, where ρ_0 is 7.3×10^{-9} eV$^{0.66}$ cm^3 s^{-1} and γ is 1.66, based on *Lotz* [1967] and *Bazylev and Chibisov* [1987].

For steady state diffusion we have [*Schulz and Lanzerotti*, 1974]

$$\frac{dT_e}{dt} = V_D \frac{dT_e}{dL} = -D_{LL}\frac{d}{dL}\ln(NL^2)\frac{dT_e}{dL} \tag{15}$$

In this case, D_{LL} is $1\times10^{-7}L^3$ s^{-1}, and the flux content NL^2 varies as $\ln L$, so we obtain

$$\frac{dT_e}{dt} = -\frac{D_{LL}}{L \ln L} \frac{dT_e}{dL} \tag{16}$$

Combining equations (16) and (14), we have now an equation governing the temperature profile of cold electrons:

$$\frac{3}{2} \frac{D_{LL}}{L \ln L} \frac{dT_e}{dL} = N_n \rho_{tor} \eta \tag{17}$$

This equation can be solved if $N_n(L)$ is assumed. Figure 13 shows a solution in which $N_n = 0$ for L<8 and $N_n = 60/\eta$ cm^{-3} for L>8. The smooth curve fits the outbound electron temperature data very well. The inbound data are better fit if we set the boundary of the neutral torus at L=9.5 and use the same neutral density. The inbound-outbound asymmetry may be a longitudinal effect, since the torus is at different L shell values at different longitudes.

The neutral hydrogen density N_n is sensitive to the value of η. The fraction of time spent by electrons in the neutral torus is approximately equal to the fraction of the flux tube volume occupied by the neutral cloud. The full thickness of the neutral torus is about 2 R_N. The flux tube cross section varies as $\cos^7\lambda$ where λ is the latitude; thus $\eta \approx 0.2$, which corresponds to a neutral hydrogen density of 300 cm^{-3}. A cloud this dense may emit enough Lyman α emission to be detected by the ultraviolet spectrometer experiment [*Cheng*, 1990]. However, the expected emissions are close enough to the detection threshold that factor of 2 changes in the torus thickness or H source rate would render these emissions invisible.

SUMMARY

We have presented the densities and temperatures of low-energy electrons in the magnetosphere of Neptune and its environs. The distributions of electrons are approximately Maxwellian in the magnetosheath and polar cusp region. Inside the magnetosphere, where the plasma beta is small, the planetary magnetic field controls the behavior of the plasma distributions. The electrons are not in thermal equilibrium, and their spectra can, in general, be fit with a combination of several Maxwellian distributions: one cold component and one or two hot components. The cold component, which has a temperature below 15 eV, is the dominant population, but hot electrons, although they make up only a few percent of the total density, contain a substantial fraction of the energy. The electric potential of the spacecraft was derived by combining electron and ion data and was 0 to -20 V in the cold plasma regions.

On the basis of the electron density and temperature profiles, we describe the major sources and sinks for magnetospheric plasma. Triton is a source of charged particles as well as neutral hydrogen and is the ultimate origin of most of the plasma detected in Neptune's magnetosphere. The neutral torus created by Triton probably contains primarily neutral hydrogen and has an inner boundary at about 8 R_N and an estimated thickness of 2 R_N. On the basis of a calculation of the electron cooling and ionization rates, we estimate that the neutral hydrogen torus density is about 300 cm^{-3}. Three plasma loss mechanisms are suggested by the PLS data: ring-satellite absorption, precipitation into Neptune's atmosphere, and charge exchange with Neptune's neutral corona.

The balance of plasma production, transport, and absorption enables us to derive time scales for diffusive transport using several independent methods, all of which give results consistent with a diffusion coefficient of $10^{-7}L^3$ R_N^2 s^{-1}. This diffusion coefficient implies that plasma transport in the magnetosphere of Neptune is very fast compared to that of Jupiter and Saturn. The mechanism driving such fast transport is not well understood at present. We have assumed throughout this paper that plasma transport is due to diffusion. An alternate model, solar wind driven magnetospheric convection, as proposed by *Selesnick* [1990] is worth considering, but the formulation of this model is more difficult and will be the subject of a later study.

Acknowledgments. The authors thank J. E. P. Connerney for providing the magnetic field model, A. Eviatar for providing the information about the electron cooling model used in the paper, R. L McNutt, Jr., for valuable comments on the manuscript, and N. F. Ness for permission to use the magnetic field data. We also acknowledge the

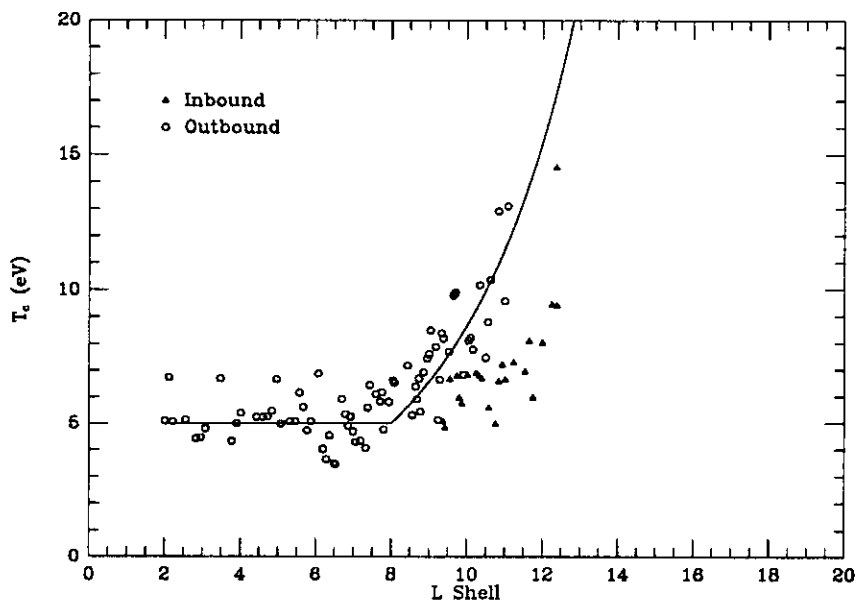


Fig. 13. The temperature of cold electrons versus the I8E1 L shell. The smooth curve is a theoretical fit to the outbound data, which requires a torus of neutral hydrogen of 300 cm^{-3} outside L=8.

leadership of the PLS team by H. S. Bridge and J. W. Belcher, without whom this study would not have been possible. This work was supported by NASA under contract 957781 from JPL to MIT and NDAP grants; M. Zhang was also partially supported by NASA grant NAGW-1209; E. C. Sittler, Jr., was supported by NASA under the Neptune Data Analysis Program.

The Editor thanks T. P. Armstrong and R. Selesnick for their assistance in evaluating this paper.

REFERENCES

Bazylev, V. A., and M. I. Chibisov, Excitation and ionization of multiply charged ions by electrons, in *Reviews of Plasma Physics, 12*, edited by M. A. Leontovich and B. B. Kadomtsev, translated from Russian by D. H. McNeill, Consultants Bureau, New York, 1987.

Belcher, J. W., et al., Plasma observations near Neptune: Initial results from Voyager 2, *Science, 246*, 1478–1482, 1989.

Bevington, P. R., *Data Reduction and Error Analysis for the Physical Sciences*, McGraw-Hill, New York, 1969.

Bridge, H. S., J. W. Belcher, R. J. Butler, A. J. Lazarus, A. M. Mavretic, J. D. Sullivan, G. L. Siscoe, and V. M. Vasyliunas, The plasma experiment on the 1977 Voyager mission, *Space Sci. Rev., 21*, 259–287, 1977.

Broadfoot, A. L., et al., Ultraviolet spectrometer observations of Neptune and Triton, *Science, 246*, 1459–1466, 1989.

Cheng, A. F., Triton torus and Neptune aurora, *Geophys. Res. Lett., 17*, 1669–1672, 1990.

Connerney, J. E. P., M. H. Acuna, and N. F. Ness, The magnetic field of Neptune, *J. Geophys. Res.*, this issue.

Coroniti, F. V., Energetic electrons in Jupiter's magnetosphere, *Astrophys. J. Suppl. Ser., 27*, 261–281, 1974.

Fälthammar, C.-G., Radial diffusion by violation of the third adiabatic invariant, in *Earth's Particles and Fields*, edited by B. M. McCormac, pp. 387–395, Reinhold, New York, 1968.

Gurnett, D. A., et al., First plasma wave observation at Neptune, *Science, 246*, 1494–1497, 1989.

Hill, T. W., and F. C. Michel, Heavy ions from the Galilean satellites and the centrifugal distortion of the Jovian magnetosphere, *J. Geophys. Res., 81*, 4561–4565, 1976.

Huebner, W. F., and P. T. Giguere, A model of comet comae, II, Effects of solar photodissociative ionization, *Astrophys. J., 238*, 753-762, 1980.

Krimigis, S. M., and T. P. Armstrong, Two-component proton spectra in the inner Saturnian magnetosphere, *Geophys. Res. Lett., 9*, 1143–1146, 1982.

Krimigis, S. M., B. H. Mauk, A. F. Cheng, E. P. Keath, M. Kane, T. P. Armstrong, G. Gloeckler, and L. J. Lanzerotti, Hot plasma parameters in Neptune's magnetosphere, *Geophys. Res. Lett., 17*, 1685–1688, 1990.

Lazarus, A. J., T. Hasegawa, and F. Bagenal, Long-lived particulate or gaseous structure in Saturn's outer magnetosphere?, *Nature, 302*, 230–232, 1983.

Lotz, W., Electron-impact ionization cross sections and ionization rate coefficients for atoms and ions, *Astrophys. J. Suppl. Ser., 14*, 207–238, 1967.

Mauk, B. H., M. Kane, E. P. Keath, A. F. Cheng, S. M. Krimigis, T. P. Armstrong, and N. F. Ness, Energetic charged particle angular distributions near ($r \leq 2\ R_N$) and over the pole of Neptune, *Geophys. Res. Lett., 17*, 1701–1704, 1990.

McNutt, R. L., Jr., R. Selesnick, and J. Richardson, Low-energy plasma observations in the magnetosphere of Uranus, *J. Geophys. Res., 92*, 4399–4410, 1987.

Moses, S. L., F. V. Coroniti, C. F. Kennel, W. S. Kurth, and D. A. Gurnett, Comparison of plasma wave measurement in the bow shocks at Earth, Jupiter, Saturn, Uranus and Neptune, *Geophys. Res. Lett., 17*, 1653–1656, 1990.

Ness, N. F., M. H. Acuna, L. F. Burlaga, J. E. P. Connerney, R. P. Lepping, and F. M. Neubauer, Magnetic fields at Neptune, *Science, 246*, 1473–1478, 1989.

Richardson, J. D., and E. C. Sittler, Jr., A plasma density model for Saturn based on Voyager observations, *J. Geophys. Res., 95*, 12,019–12,031, 1990.

Richardson, J. D., A. Eviatar, and M. L. Delitsky, The Triton torus revisited, *Geophys. Res. Lett., 17*, 1673–1676, 1990.

Richardson, J. D., J. W. Belcher, M. Zhang, and R. L. McNutt, Jr., Low-energy ions near Neptune, *J. Geophys. Res.*, this issue.

Schulz, M., and L. J. Lanzerotti, *Particle Diffusion in the Radiation Belts*, Springer-Verlag, New York, 1974.

Scudder, J. D., E. C. Sittler, Jr., and H. S. Bridge, A survey of the plasma electron environment of Jupiter: A view from Voyager, *J. Geophys. Res., 86*, 8319–8342, 1981.

Selesnick, R. S., Plasma convection in Neptune's magnetosphere, *Geophys. Res. Lett., 17*, 1681–1684, 1990.

Simpson, J. A., T. S. Bastian, D. L. Chenette, R. B. McKibben, and K. R. Pyle, The trapped radiations of Saturn and their absorption by satellites and rings, *J. Geophys. Res., 85*, 5731–5762, 1980.

Siscoe, G. L., Towards a comparative theory of magnetospheres, in *Solar System Plasma Physics*, vol. II, edited by C. F. Kennel, L. J. Lanzerotti, and E. N. Parker, pp. 319–402, North-Holland, Amsterdam, 1979.

Sittler, E. C., Jr., Plasma electron analysis: Voyager plasma science experiment, *NASA Tech. Memo., 85037*, 1983.

Sittler, E. C., Jr., and D. F. Strobel, Io plasma torus electrons: Voyager 1, *J. Geophys. Res., 92*, 5741–5762, 1987.

Sittler, E. C., Jr., J. D. Scudder, and H. S. Bridge, Distribution of neutral gas and dust near Saturn, *Nature, 292*, 711–714, 1981.

Sittler, E. C., Jr., K. W. Ogilvie, and J. D. Scudder, Survey of low-energy plasma electrons in Saturn's magnetosphere, *J. Geophys. Res., 88*, 8848–8870, 1983.

Sittler, E. C., Jr., K. W. Ogilvie, and R. S. Selesnick, Survey of electrons in the Uranian magnetosphere: Voyager 2 observations, *J. Geophys. Res., 92*, 15,263-15,281, 1987.

Smith, B. A., et al., Voyager 2 at Neptune: Imaging science results, *Science, 246*, 1422–1449, 1989.

Spreiter, J. R., and S. S. Stahara, A new predictive model for determining solar wind-terrestrial planet interactions, *J. Geophys. Res., 85*, 6769–6777, 1980.

Stone, E. C., A. C. Cummings, M. D. Looper, R. S. Selesnick, N. Lal, F. B. McDonald, J. H. Trainor, and D. L. Chenette, Energetic charged particles in the magnetosphere of Neptune, *Science, 246*, 1498–1494, 1989.

Szabo, A., A. J. Lazarus, R. L. McNutt, Jr., G. L. Siscoe, R. P. Lepping, and N. F. Ness, Magnetopause and cusp observations at Neptune, *J. Geophys. Res.*, this issue.

Tyler, G. L., et al., Voyager radio science observations of Neptune and Triton, *Science, 246*, 1466–1473, 1989.

Van Allen, J. A., Absorption of energetic protons by Saturn's ring G, *J. Geophys. Res., 88*, 6911–6918, 1983.

Van Allen, J. A., M. F. Thomsen, B. A. Randall, R. L. Rairden, and C. L. Grosskreutz, Saturn's magnetosphere, rings and inner satellites, *Science, 207*, 415–421, 1980.

Yung, Y. L., and J. R. Lyons, Triton: Topside ionosphere and nitrogen escape, *Geophys. Res. Lett., 17*, 1717–1720, 1990.

J. D. Richardson, Center for Space Research, MIT, Cambridge, MA 02139.

E. C. Sittler, Jr., NASA Goddard Space Flight Center, Code 692, Greenbelt, MD 20771.

M. Zhang, the Enrico Fermi Institute, the University of Chicago, Chicago, IL 60637.

(Received April 18, 1991;
revised June 29, 1991;
accepted July 15, 1991.)